A universal approach to predicting resilience of complex systems

Mengkai Xu
Northeastern University
Srinivasan Radhakrishnan
Northeastern University
Xiaoning Jin
Northeastern University
Sagar Kamarthi (shen494157765@gmail.com)
Northeastern University

Physics Article

Keywords:

Posted Date: March 18th, 2022

DOI: https://doi.org/10.21203/rs.3.rs-1325130/v1

A Universal Approach to Predicting Resilience of Complex Systems

Mengkai Xu[1], Srinivasan Radhakrishnan[1], Xiaoning Jin[1], Sagar Kamarthi[1*]

[1]Mechanical and Industrial Engineering Department, Northeastern University

360 Huntington Ave., Boston, Massachusetts 02115 , USA

[*]To whom correspondence should be addressed; E-mail: s.kamarthi@northeastern.edu

October 29, 2021

Abstract

Dynamical complex systems such as ecosystems, biological systems, economic systems and technological infrastructures thrive on their networked components. Their resilience depends on their ability to recover from the impact of perturbations. Due to complex interactions among components in the networked systems, perturbations could cause cascading failures, consequently instability, and eventually collapse of the systems. Theoretical studies have been far from successful in predicting these events because of the high-dimensional structure of interacting components. The studies on complex systems have yet to fully explore the occurrences of state transition, systemic collapse, and impact of structural properties on resilience. In this work, we address these longstanding theoretical issues. We derive a set of formulations that help us understand the mechanism of high-dimensional interactions among components and uncover the principles that control the dynamics of interacting components. Our formulation reduces the system's high dimensional dynamics to a parsimonious resilience function of a parameter that solely depends on the topology but effectively captures the complex interaction structure. The experimental results demonstrate that the formulation can accurately predict the resilience loss brought about by perturbations and identify the tipping point where the systemic collapse occurs. These predictive results can be used for enhancing a complex system's ability to withstand perturbations and avert catastrophic collapses. The

study highlights the topological properties that can be used as principles for improving the resilience of ecosystems, biological systems, economic systems and technological infrastructures.

Introduction

Resilience is an intrinsic property of a complex system that defines its ability to maintain basic functionality when subjected to perturbations [1,2]. Resilience is generally characterized by the state of the system [3]. The structural parameters of the system inherently determine the stable fixed point of the nonlinear dynamical equations governing the system dynamics [1,4,5]. Perturbations disrupt the topological structure of interactive components and consequently cause a state transition of the system [6–9]. As perturbed components terminate their interactions with their neighbors, the system transits into a new state which is often an unstable and undesirable state. This adversely affects the functionality of the system at the local or global scale and alter the system resilience [10–13]. Such system transition from a desired state to an undesired state results in its resilience loss [1]. Perturbations commonly induce cascading failures, leading to collapses of many complex systems [4,12,14–20]. Despite the widespread impacts of systemic collapses, they are mostly unpredictable [1,5,16]. In addition, the efforts to uncover the rules of state transitions have been challenging due to the high dimensionality of dynamical equations [1,3,5,14,16,21]. We address these issues by deriving a formulation that reduces the dimension of system dynamics. Our main contribution is a parsimonious resilience function built on a single topology-dependent parameter that effectively captures the complex interaction structure. This compact resilience function helps us identify the determinant structural properties that affect both the system resilience and the transition tipping point. We show the formulation is effective in predicting the resilience of a variety of complex systems, including mutualistic ecological, biological and technological networks, which are characterized by very different functional forms of interactions and distinct topological structures. The analytical results also provide insights for designing resilient networked systems.

Resilience function of complex systems

A complex dynamical system is represented as a network comprising of N components (nodes) whose activities $\mathbf{x} = (x_1, ..., x_N)^\top$ are expressed by the following coupled nonlinear equation [1,4,20]

$$\frac{dx_i}{dt} = F(x_i) + \sum_{j=1}^{N} A_{ij} G(x_i, x_j) \tag{1}$$

where the first term $F(x_i)$ expresses the intrinsic dynamics of node i; the second term expresses the interaction dynamics between node i and other nodes interacting with it; the interaction function $G(x_i, x_j)$ represents the nature of interactions; and the structural parameter A_{ij}, known as topology, represents the pairwise interaction strength between nodes i and j. Given the specific forms of $F(x_i)$ and $G(x_i, x_j)$, the state of the system featured by the stable fixed-point x_i^c in Eq. (1) is used to describe the resilience of many complex systems including ecosystems [21,22], biological networks [1,5,23] and technological infrastructures [24] (Fig. 1a). Interactions generally take diverse forms across these disparate systems, and their topology A_{ij} is determined by the interaction structure of the network, and whether the interactions are directed or undirected [1,4,23,24]. The dynamics of the network is intrinsically determined by the structure of node interactions, wherein the state of each node is directly affected by the state of its immediate adjacent nodes. In this sense, each node acts as an intermediary facilitating indirect interactions between its immediate neighbors (dashed curve in Fig. 1b). The stable state of each node, as the consequence of interactions, is determined by the interaction structure (Fig.1c). Resilience loss of a complex system is attributed to the changes in the $N \times N$ parameter space defined by A_{ij}. The changes commonly take place as one or more nodes transition from a functional state to a non-functional state [1,4]. The main challenge of using dynamic equation in the form of Eq. (1) is its high dimensionality, which prohibits an effective analysis to gain meaningful insights into the mechanism of state transitions and predict the occurrence of the tipping point and future system state.

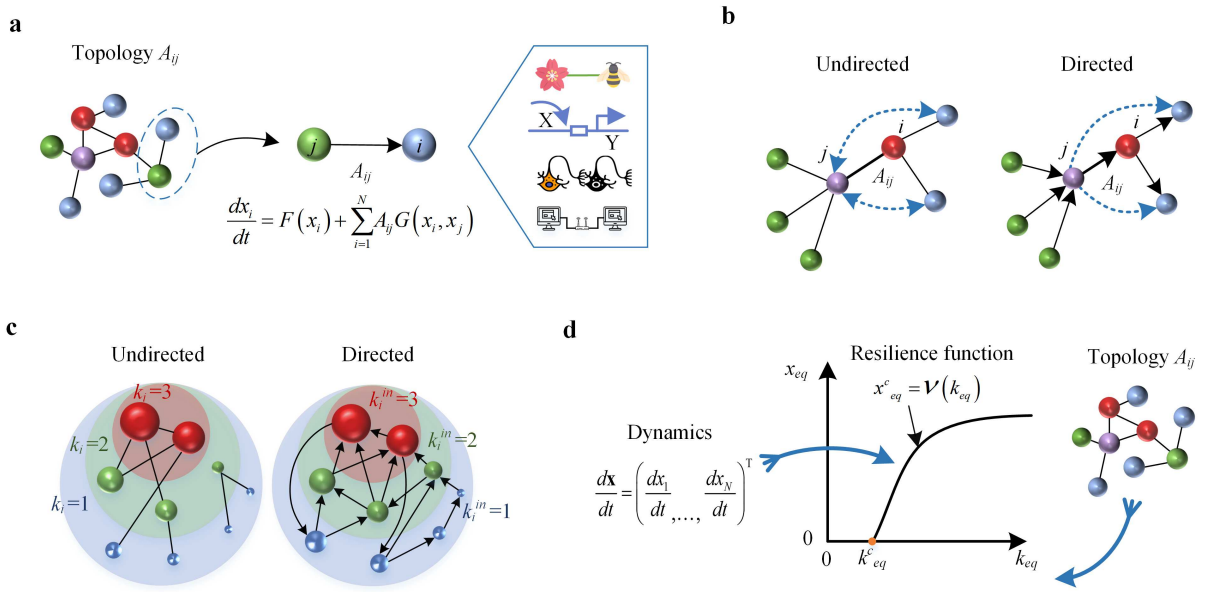

Figure 1: **Resilience of complex systems**. **a**, The differential equation captures the resilience of high-dimensional complex systems which are governed by the intrinsic dynamics $F(x_i)$ of nodes and interactions $A_{ij}G(x_i, x_j)$ between nodes. **b**, The structures of complex systems are generally represented by the directed or undirected networks, where the state of a node directly affects (solid lines) the state of its adjacent nodes and also forms indirect interactions (dashed lines) between its immediate neighbors. **c**, The stable states of interacting nodes in a directed or an undirected network with cooperative interactions are determined by the interaction structure, and the node size is proportional to its activity. **d**, The high-dimensional topological structure, through transformations, is reduced to a function of a single parameter k_{eq}. The high-dimensional complex systems $\left(\frac{dx_1}{dt}, \ldots, \frac{dx_N}{dt}\right)^{\top}$ shown in **a** are reduced to a single resilience function $x^c_{eq} = \mathcal{V}(k_{eq})$ in the x_{eq}-k_{eq} space; k^c_{eq} (orange dot) is the predicted critical threshold (tipping point) at which systems go through a transition from a resilient state to the irreversible state of collapse. The shape of the resilience curve and the critical threshold k^c_{eq} are uniquely determined by $F(x_i)$ and $G(x_i, x_j)$ for the specific system.

Unidimensional resilience function through analytical dimension reduction

To address this challenge, we revise the second term in Eq. (1) while preserving the original pairwise interaction dynamics:

$$\frac{dx_i}{dt} = F(x_i) + \sum_{j=1}^{N} M_{ij} Q(x_i, x_j) \tag{2}$$

Eq. (2) is equivalent to Eq. (1), whereas the former is still high-dimensional except that the weighted topological parameter A_{ij} is replaced with M_{ij}, which is an element in a (0,1)-adjacency-matrix $\boldsymbol{M}$; M_{ij} = 1 if nodes i and j interact, 0 otherwise; $Q(x_i, x_j)$ is the revised interaction term, which preserves the original interaction dynamics of Eq. (1). This reformulation relies on the fact that A_{ij} can be derived from M_{ij} [1,22]. However, the revised high-dimensional equation can neither explain nor predict the state transitions of a stable fixed point, because M_{ij} is still in the $N \times N$ space. The purpose of reformulating Eq. (1) is to simplify the representation of the interaction structure with simple topological parameters. The simplification allows us to identify the stable fixed points of Eq. (1) from the uninterpretable and unpredictable high-dimensional space to an explainable and predictable low-dimensional space. The natural law of interaction implies that the state of each node is influenced by the state of its immediate interacting nodes [1,4]. This motivates us to use the weighted average state x_{eq} to associate the states of nodes. The weighted average state x_{eq} equivalently describes the system dynamics in Eq. (1) (Supplementary Information section II). The state x_i of any node i can be effectively expressed by x_{eq}. Thus our objective of predicting x_i becomes equivalent to predicting the state x_{eq}. Upon expressing $\mathbf{x} = (x_1, ..., x_N)^\top$ by x_{eq}, the mathematical transformation presented in Supplementary Information section II shows that the N-dimensional Eq. (2) reduces to a unidimensional dynamical equation:

$$\frac{dx_{eq}}{dt} = F(x_{eq}) + Q(x_{eq}, k_{eq}) \tag{3}$$

where

$$k_{eq} = \frac{\boldsymbol{k}_{\text{out}}^\top \boldsymbol{M} \boldsymbol{k}_{\text{in}}}{\boldsymbol{k}_{\text{out}}^\top \boldsymbol{k}_{\text{in}}} \tag{4}$$

The column vectors $\boldsymbol{k_{in}} = ({k_1}^{in}, ..., {k_N}^{in})^\top$ and $\boldsymbol{k_{out}} = ({k_1}^{out}, ..., {k_N}^{out})^\top$ denote the in-degree and out-degree of N nodes respectively. Here, the complex interaction structure A_{ij} in the $N \times N$ space is condensed into a single parameter k_{eq} (Fig. 1d); any changes in the topological structure A_{ij} induced by perturbations can be captured by the corresponding changes in k_{eq}. So far, the structural complexity of the high-dimensional model Eq. (1) has been reduced to a unidimensional equation given by Eq. (3); the state of the system expressed by the stable fixed point of Eq. (3) can be derived. Through numerical stability analyses (Supplementary Information section II), the stable fixed point, x^c_{eq}, of Eq. (3), herein standing for network resilience, can be expressed as a function of k_{eq}

$$x^c_{eq} = \mathcal{V}\left(k_{eq}\right) \tag{5}$$

The expression of $\mathcal{V}\left(k_{eq}\right)$ is uniquely determined by the selection of $F(x_i)$ and $G(x_i, x_j)$ in Eq. (1). This parsimonious expression directly relates network resilience to k_{eq}. Accounting for the direction of resilience transition is not possible through Eq. (1). Fig. 1d illustrates the predicted resilience of the high-dimensional network $\left(\frac{dx_1}{dt}, ..., \frac{dx_N}{dt}\right)^\top$ with interactions (directed or undirected) can be characterized by Eq. (5), which is a function of k_{eq} in the x_{eq}-k_{eq} space. Our formulation also enables us to predict the critical threshold k^c_{eq}, beyond which the system will reach a state of collapse ($x^c_{eq} = 0$). The critical threshold k^c_{eq} is determined by the dynamical functions $F\left(x_i\right)$ and $G\left(x_i, x_j\right)$. This formulation, that maps the high-dimensional dynamics of Eq. (1) to unidimensional Eq. (5), allows us to perform simple numerical analysis to predict the resilience of a variety of complex systems.

To demonstrate the effectiveness and accuracy of resilience prediction, we test our formulation on different complex systems: (i) mutualistic ecological, (ii) gene regulatory, and (iii) brain neural. These systems are governed by different laws of dynamics and characterized by different topological structures determined by the interactive patterns between their components.

Numerical study of resilience of mutualistic ecological networks

We first investigate mutualistic ecological networks, which exhibit high dimensionality in mutual interactions of species. The dynamics of abundance x_i of species i in a mutualistic ecological network, following Eq. (1), is described as[21,22]

$$\frac{dx_i}{dt} = -gx_i - sx_i^2 + \frac{x_i \sum_{j=1}^{N} A_{ij}x_j}{1 + h\sum_{j=1}^{N} A_{ij}x_j} \tag{6}$$

The first term stands for the growth of species i at a rate g; the second term describes the internal competition with a self-limitation parameter s; the third term represents the mutualistic interaction between species i and species j; h is the saturation constant that limits the mutualistic benefit; and A_{ij} is the mutualistic interaction strength between species i and j, and can be calculated as:

$$A_{ij} = \frac{\gamma_o M_{ij}}{k_i^{\delta}} = \frac{\gamma_o M_{ij}}{\left(\sum_{j=1}^{N} M_{ij}\right)^{\delta}} \tag{7}$$

where $\gamma_o = 1$ denotes the level of mutualistic interaction strength; $M_{ij} = 1$ if species i and j interact, $M_{ij} = 0$ otherwise; k_i is the number of species with which species i interacts; and δ ($0 \leq \delta \leq 1$) represents the trade-off between interaction strength and number of interactions. Species in mutualistic ecological networks follow undirected interactions (Fig. 1c), hence they have a symmetric interaction structure M_{ij} = M_{ji}.

We use Eq. (6) to investigate the resilience profiles of fourteen empirical mutualistic ecological networks (N1-N14) with different topological structures that capture the symbiotic interactions between species (Supplementary Information Table 1). The number of species N of these networks ranges from 36 to 1,884. The parameters in Eq. (6) are set to $s = 0.4$, $h = 0.5$, $g = 0.3$, $\gamma_o = 1$, and $\delta = 0.5$. To simulate the realistic perturbations in ecosystem, we implemented 200 realizations by randomly removing a fraction f_n of species, which indicates the level of severity of perturbations. In each instance of species removal, we use Eq. (6) to compute the equivalent average abundance x_{eq} of all species. The results across 200 realizations are presented in Supplementary Information, Fig. S1 and Fig. S2. The results demonstrate the abundance of species, x_{eq}, for these fourteen networks against the fraction f_n of species removal. The figures indicate that species for all networks remain abundant against

small perturbations (small f_n) and become less abundant when f_n becomes large. When the perturbation exceeds a specific threshold, the tipping point of collapse emerges. We observe that each network displays a range of tipping points for different degree of species removal. For example, the tipping points for network N1 vary from 53% to 97% of species removal; this range for network N8 is between 67% and 99% (Supplementary Information Fig. S1). These results indicate that the same form of perturbations can lead to different outcomes for the same complex system. These fourteen ecological networks (i.e., N - N14) also display different resilience loss profiles against perturbations. The tipping points vary significantly across these networks. For example, network N5 does not collapse until at least 97% of species are removed (Supplementary Information Fig. S1); network N13 collapses when over 47% of species are removed (Supplementary Fig. S2). The differences are actually rooted in the diversity of topological structures of these networks. Fig. 2b-o show the average of 200 realizations for the fourteen networks (i.e., N - N14), each having a unique resilience profile.

The diverse resilience transition patterns and ranges of tipping points at different degree of species removal across networks reveal that it is difficult to generalize the prediction of the exact trend of resilience transition and the emergence of a tipping point (Supplementary Information Fig. S1-S2). We now show that these obstacles can be overcome by our formulation presented by Eq. (2)-(5). Following the principles that govern the system's dynamics, Supplementary Information section III describes the stability analysis for reducing the high-dimensional model Eq. (6) to a parsimonious function.

$$x_{eq}^{c} = \frac{ghk_{eq}^{1-\delta} + s - k_{eq}^{1-\delta} - \left[\left(ghk_{eq}^{1-\delta} + s - k_{eq}^{1-\delta}\right)^2 - 4gshk_{eq}^{1-\delta}\right]^{\frac{1}{2}}}{-2hsk_{eq}^{1-\delta}} \Theta\left(k_{eq} - k_{eq}^{c}\right) \tag{8}$$

where x_{eq}^{c} is the stable fixed point, which is equivalent to the average of species abundance of the ecological network. The critical threshold below which the network suffers an irreversible collapse is predicted as $k_{eq}^{c} = \left[\frac{(\sqrt{gh}-1)^2}{s}\right]^{\frac{1}{\delta-1}}$, which follows only the function parameters in Eq. (6) and is independent of the network topology. Here $\Theta\left(k_{eq} - k_{eq}^{c}\right)$ is a logic function that indicates the occurrence of network collapse, where $\Theta\left(k_{eq} - k_{eq}^{c}\right) = 1$ if $k_{eq} \geq k_{eq}^{c}$, 0 otherwise. Given the previously configured function parameters, k_{eq}^{c} can be calculated and is 1.14

for all the networks. Eq. (8) can be regarded as the predicted resilience function in the form $x_{eq}^{c} = \mathcal{V}(k_{eq})$ (Fig. 1d). The transition between different states for all the ecological networks can be analytically predicted by Eq. (8).

Now we can map the data from all the realizations presented in Supplementary Information Fig. S1-S2 to the x_{eq}-k_{eq} space (see Fig. 2p). We show that all data points are located on or close to this universal resilience curve, irrespective of the diverse responses of networks to perturbations. More importantly, the tipping points across all ecological networks are invariantly predicted to be at k_{eq}^{c} in the x_{eq}-k_{eq} space, showing that the collapse always occurs at k_{eq}^{c} for all networks. In order to show the prediction consistency of our formulation, we further validate that the diverse resilience profile of each individual network can also be predicted in the x_{eq}-f_n space. The predicted results of our formulation are shown as the black curves in Fig. 2b-o. These analytical findings strongly indicate that our predicted resilience function Eq. (8) is universally effective across networks with different topological structures. Additional testing of this generalizability on networks with more complex topological structures is presented in Supplementary Information section IX.

In practice, high-dimensional models of system dynamics prohibit them from being practically used to predict the state transition and the tipping point. Our formulation describes the high-dimensional systems with a single resilience function in the x_{eq}-k_{eq} space. This resilience function accurately predicts not only the direction of state transitions for a range of perturbations but also the critical tipping point where the networks collapse into an irreversible non-resilient state.

Numerical study of resilience of gene regulatory networks

Next we investigate the resilience of gene regulatory networks, which describes the directed regulatory transcription interactions between genes[23]. According to Eq. (1), the dynamics of gene expression x_i in terms of the amount of protein produced are governed by the Michaelis-Menten equation[1,5,23]

$$\frac{dx_i}{dt} = -mx_i^f + \sum_{j=1}^{N} A_{ij} \frac{x_j^n}{\alpha^n + x_j^n} \tag{9}$$

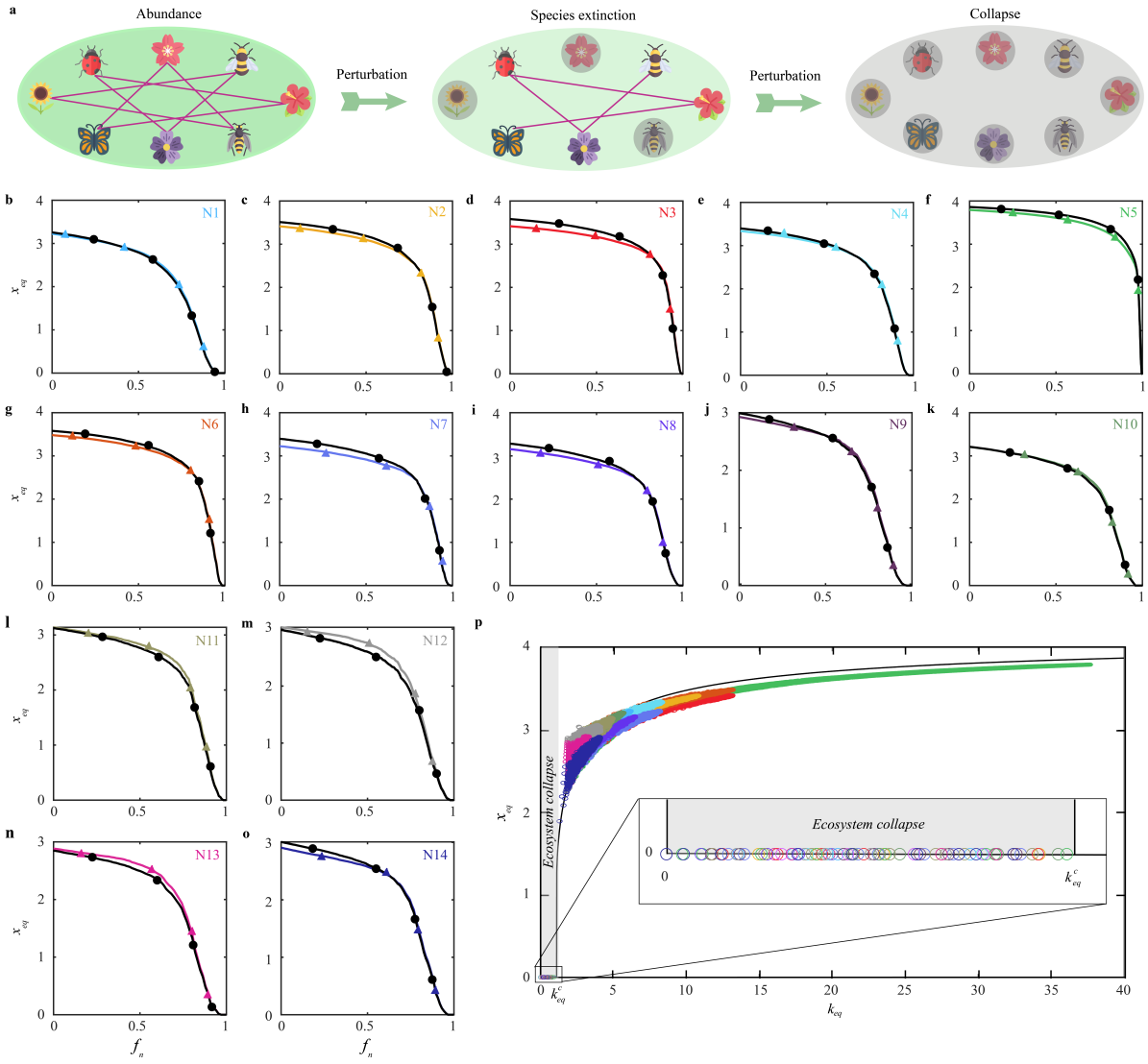

Figure 2: **Resilience of mutualistic ecological networks**. **a,** In ecosystems, the realistic perturbation naturally occurs in the form of species removal; links between surviving species and extinct (removed) species are disconnected accordingly. **b-o,** The equivalent average species abundance x_{eq} versus the fraction f_n of species removed for fourteen empirical ecological networks. Curves with different colors represent the average of 200 random realizations calculated by Eq. (6). In Supplementary Information Fig. S1 and Fig. S2, black curves show the results predicted by Eq. (8). **p,** The black curve, denoting the resilience function for mutualistic ecological networks, is predicted by Eq. (8). The data points calculated by Eq. (6) for fourteen diverse empirical ecological networks shown in Supplementary Information Fig. S1 and Fig. S2 are projected onto the x_{eq}-k_{eq} space. The results indicate that regardless of the diversity of network structure and the responses to perturbations, the state of the network is accurately predicted by Eq. (8).

where m is the mortality rate; f is a parameter that describes degradation or dimerization; A_{ij} is the maximal interaction strength between genes i and j; here $A_{ij} = \gamma M_{ij}$, where γ is a positive activation coefficient; n is the Hill coefficient capturing the steepness of the Hill function; and α is the activation coefficient. Unlike the undirected structure in mutualistic ecological networks, the high-dimensional interactions in gene regulatory networks are directed and asymmetric (Fig. 1c), indicating that a regulated gene generally does not regulate the states of its regulating genes, $M_{ij} \neq M_{ji}$. Selecting the parameters f =1, m = 1, $\gamma = 2$, $n = 2$, and $\alpha = 1$, two gene regulatory networks *Saccharomyces Cerevisiae*[1] and *Escherichia Coli*[25] are numerically studied by subjecting them to random gene removal to a varying degree (see Supplementary Information section V). The responses of these two networks to perturbations in 200 realizations are shown in Supplementary Information Fig. S9. Analogous to mutualistic ecological networks, gene regulatory networks remain highly active under small perturbations and undergo a critical transition to the collapse state when perturbations are sufficiently severe. Likewise, gene regulatory networks exhibit diverse resilience loss patterns and divergent tipping points in the x_{eq}-f_n space, where the resilience transitions and the emergence of network collapse are unpredictable. By taking the average of all the realizations, we show the the resilience profile of each regulatory network in Fig. 3a-b. In compliance with our formulation from Eq. (2) to Eq. (5), the high-dimensional model in Eq. (9) is reduced to a parsimonious resilience function (Supplementary Information section V)

$$x_{eq}^{c} = \frac{\gamma k_{eq} + \sqrt{\gamma^2 k_{eq}^2 - 4\alpha^2 m^2}}{2m} \Theta\left(k_{eq} - k_{eq}^{c}\right) \tag{10}$$

where x_{eq}^{c} is the stable fixed point, representing the equivalent average gene expression of the network. In the logic function $\Theta\left(k_{eq} - k_{eq}^{c}\right)$, the critical threshold is predicted as $k_{eq}^{c} = \left[\frac{m\alpha^n}{\gamma(\gamma(n-f)/mn)^{\frac{n-f}{f}} - m(\gamma(n-f)/mn)^{\frac{n}{f}}}\right]^{\frac{f}{n}}$. The parameter k_{eq}^{c} relies solely on the function parameters in Eq. (9); here the critical threshold happens to be at k_{eq}^{c} = 1. This parsimonious expression in Eq. (10) predicts a resilience function of the form given in Fig. 1d, characterizing a single resilience curve for gene regulatory networks (black curve in Fig. 3c). By mapping the data in Supplementary Information Fig. S9 into the x_{eq}-k_{eq} space, we observe that all data points lie on the resilience curve (see Fig. 3c), regardless of the diverse responses of these two regulatory networks to perturbations. From

the results predicted by our model in the x_{eq}-f_n space (black curve in Fig. 3a-b), we observe that the resilience profiles predicted by our model are consistently accurate.

Numerical study of resilience of brain neural networks

Lastly we investigate resilience of brain neural networks where neurons interact through directed electrical activities. The dynamics of the membrane potential x_i of neuron i in brain neural networks is modeled as[5,26]

$$\frac{dx_i}{dt} = I - \frac{x_i}{R} + \frac{1}{2}\sum_{j=1}^{N} A_{ij} \tanh\left[n\left(x_j - \alpha\right)\right] \tag{11}$$

where I is the basal activity; R is the inverse of the death rate; A_{ij} is the synaptic efficacy denoting the maximum interaction strength from neuron j to i, wherein $A_{ij} = \gamma M_{ij}$; α is the firing threshold; the coefficient n describes the level of cooperation governed by the steepness of the interaction. Although interactions between neurons in brain neural networks are directed, unlike gene regulatory networks, the state of a neuron in some cases affects the state of neurons which influence its state, indicating that neural networks are partially symmetric. Selecting the parameters $I = 0.5$, $R = 2$, $J = 2$, $\alpha = 1$, $\gamma = 2$ and $n = 1$, two brain neural networks *C.elegans Frontal* and *C.elegans Global*[27,28] are numerically studied by subjecting them to random neural removal to a varying degree. The responses to perturbations of these two networks are examined in 200 realizations (see Supplementary Information Fig. S10). Similar to ecological and regulatory networks, neural networks remain resistant to small perturbations and undergo a critical transition to the collapse state only when perturbations are large. The diversity of resilience loss and collapse patterns are also observed in the x_{eq}-f_n space (Supplementary Information Fig. S10), showing the unpredictable nature of resilience transitions in neural networks. The unique resilience profile of each neural network depicted by the average of all the realizations are presented in Fig. 3d-e. In accordance with our formulation, Eq. (2) through Eq. (5), the high-dimensional model Eq. (11) is reduced to a parsimonious resilience expression (Supplementary Information section VI)

$$x_{eq}^{c} \approx \left(RI + \frac{R\gamma k_{eq}}{2} \right) \Theta \left(k_{eq} - k_{eq}^{c} \right) \tag{12}$$

where x_{eq}^{c} is the stable fixed point, representing the equivalent average state of the neural network. In the logic function $\Theta \left(k_{eq} - k_{eq}^{c} \right)$, the critical threshold is predicted to be $k_{eq}^{c} = \frac{2}{Rn\gamma}$. The parameter k_{eq}^{c} relies solely on the function parameters in Eq. (11); here the critical threshold is predicted to be k_{eq}^{c} = 0.5. This parsimonious function Eq. (12) predicts the resilience of the system in the form presented in Fig. 1d, featuring a single resilience curve for neural networks (black curve in Fig. 3f). The data plotted in the x_{eq}-k_{eq} space in Supplementary Information Fig. S10, show that all data points are on or near this resilience curve (see Fig. 3f) regardless of the diversity observed in Supplementary Information Fig. S10. The results predicted by Eq. (12) in the x_{eq}-f_n space (black curve in Fig. 3d-e) also attest the prediction consistency of our model.

Effects of topological properties on resilience

Based on the analysis of networks with different topological structures and properties, we demonstrate the effectiveness and universality of our method in predicting the resilience of a broad range of complex network systems in spite of heterogeneity of network structure. The universality is attributed to the simplicity of the dynamic functions $F(x_i)$ and $G(x_i, x_j)$ which uniquely delineate the resilience prediction function $\mathcal{V}$. The actual state of the system derived from the resilience function is determined by the network topology M_{ij}, as expressed through k_{eq} in Eq. (4). To further understand the impact of topological characteristics on network resilience, k_{eq} is expressed as the product of four determinant topological characteristics.

$$k_{eq} = \hat{\boldsymbol{D}} \cdot \hat{\boldsymbol{R}} \cdot \hat{\boldsymbol{P}} \cdot \hat{\boldsymbol{S}} \tag{13}$$

where $\hat{\boldsymbol{D}} = E/N$ indicates the network density defined as the ratio between the number of links E and the number of nodes N; network assortativity $\hat{\boldsymbol{R}} = 2\boldsymbol{k}_{\text{out}}^{\top}\boldsymbol{M}\boldsymbol{k}_{\text{in}} / \| \boldsymbol{M} \left(\boldsymbol{k}_{\text{out}}\boldsymbol{k}_{\text{out}}^{\top} + \boldsymbol{k}_{\text{in}}\boldsymbol{k}_{\text{in}}^{\top} \right) \|$ measures the association between in-degree and out-degree of all nodes, $0 < \hat{\boldsymbol{R}} \leq 1$; $\hat{\boldsymbol{P}} = N\|\boldsymbol{M} \left(\boldsymbol{k}_{\text{out}}\boldsymbol{k}_{\text{out}}^{\top} + \boldsymbol{k}_{\text{in}}\boldsymbol{k}_{\text{in}}^{\top} \right) \| / 2\boldsymbol{k}_{\text{in}}^{\top}\boldsymbol{k}_{\text{out}} \| \boldsymbol{M} \|$ represents

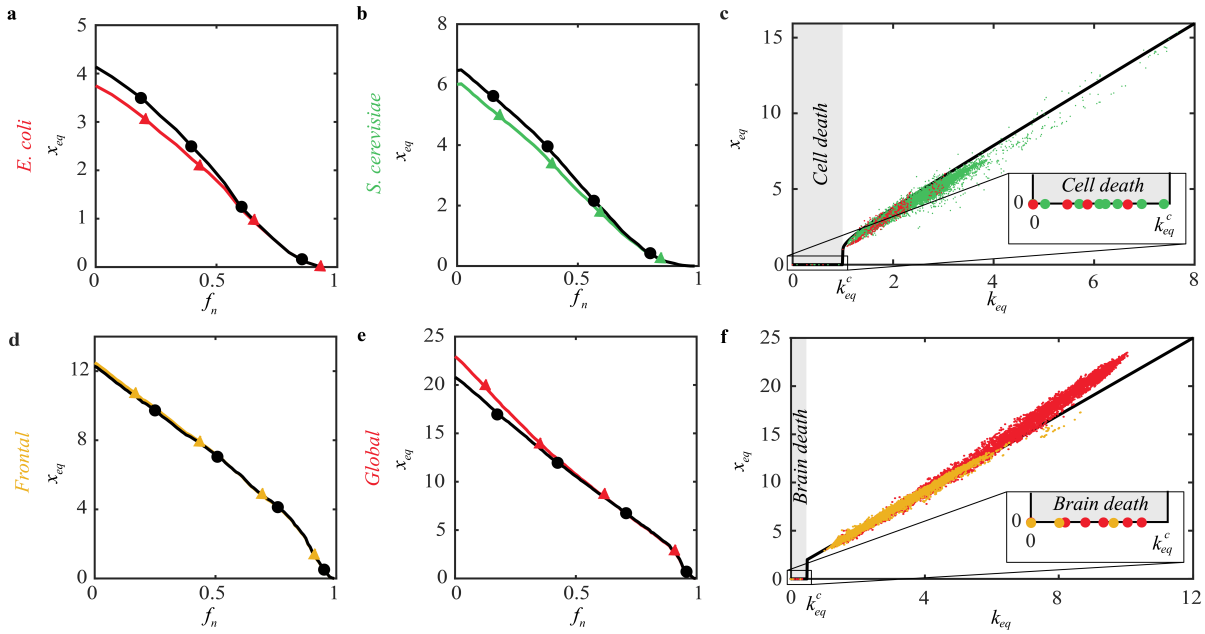

Figure 3: **Resilience of gene regulatory network and brain neural network**. **a-b,** The resilience profile, which is the average of 200 realizations calculated by Eq. (9), is shown in Supplementary Information Fig. S9; it displays the equivalent average gene expression x_{eq} versus f_n for two gene regulatory networks (red and green). Black curves are the results predicted by Eq. (10). **c,** The black curve, which indicate the resilience function for regulatory networks, is predicted by Eq. (10). The data points calculated by Eq. (9) in Supplementary Information Fig. S9 for two regulatory networks are projected onto the x_{eq}-k_{eq} space. **d-e,** The resilience profile, which is the average of 200 realizations calculated by Eq. (11), is shown in Supplementary Information Fig. S10; it displays the equivalent average membrane potential x_{eq} versus f_n for two neural networks (yellow and red). Black curves represent the results predicted by Eq. (12). **f,** The black curve, which indicates the resilience function for neural networks, is predicted by Eq. (12). The data points calculated by Eq. (11) in Supplementary Information Fig. S10 for two neural networks are projected onto the x_{eq}-k_{eq} space. Regardless of the diversity of network structures and the responses to perturbations, the state of the system can be accurately predicted by the corresponding resilience function for the specific system.

the distribution of node degree that indicates the heterogeneity of degree distribution; $\hat{\boldsymbol{S}} = \|\boldsymbol{M}\|/E$ indicates the directedness of the network; here, $\hat{\boldsymbol{S}} = 1$ for directed networks and $\hat{\boldsymbol{S}} = 2$ for undirected networks (Fig. 4 a-d). The details of derivation of k_{eq} are presented in Supplementary Information section VIII. The relationship between k_{eq} and the four topological properties indicates that an undirected network with high density, high heterogeneity, and high assortativity has a large k_{eq}.

Equation (13) helps us identify the network characteristics that can improve a system's resilience. The results shown in Fig. 2 and Fig. 3 indicate that the greater the k_{eq}, the higher the system resilience. We visualize the topological characteristics of all the networks studied in three 2D plots, Fig. 4e-4g, whose coordinates are $\hat{\boldsymbol{D}} \cdot \hat{\boldsymbol{S}}, \hat{\boldsymbol{P}}$ and $\hat{\boldsymbol{R}}$. These figures reveal that the source of resilience of each network is different; for example, the resilience of network N2 is mainly attributed to its high assortativity; network N5 has high resilience due to its high density and assortativity; and resilience of N12 is attributed to its heterogeneity. To test the effect of heterogeneity and assortativity on undirected networks, we deliberately construct two synthetic networks: one with no heterogeneity (i.e. homogeneous network) and another with high assortativity while keeping all other characteristics the same as those for N12. As can be seen in Fig. 4h, the reduction of heterogeneity pushes the constructed homogeneous network into a collapse state, while the rise of assortativity greatly increases the endurance of the network against perturbations. By analyzing directed networks, the source of *Saccharomyces Cerevisiae*'s resiliece is its high density relative to the density of *Escherichia Coli*; and the sources of *C.elegans Global*'s resilience are its high density and high heterogeneity relative to those of *C.elegans Frontal*. To test the effects of assortativity and heterogeneity in directed networks, we modify *C.elegans Global* network by decreasing its assortativity and increasing its heterogeneity while preserving all other characteristics the same as those for the two directed networks respectively. The analytical results in Fig. 4i show that a heterogeneous directed network with high assortativity is more resilient than a homogeneous directed network with low assortativity. Undirected ecological networks tend to be more resilient than directed gene regulatory and brain neural networks. Among all the directed networks tested, brain neural networks, which are partially symmetric with high density, are more resilient than asymmetric gene regulatory networks. These four characteristics of each network are included in

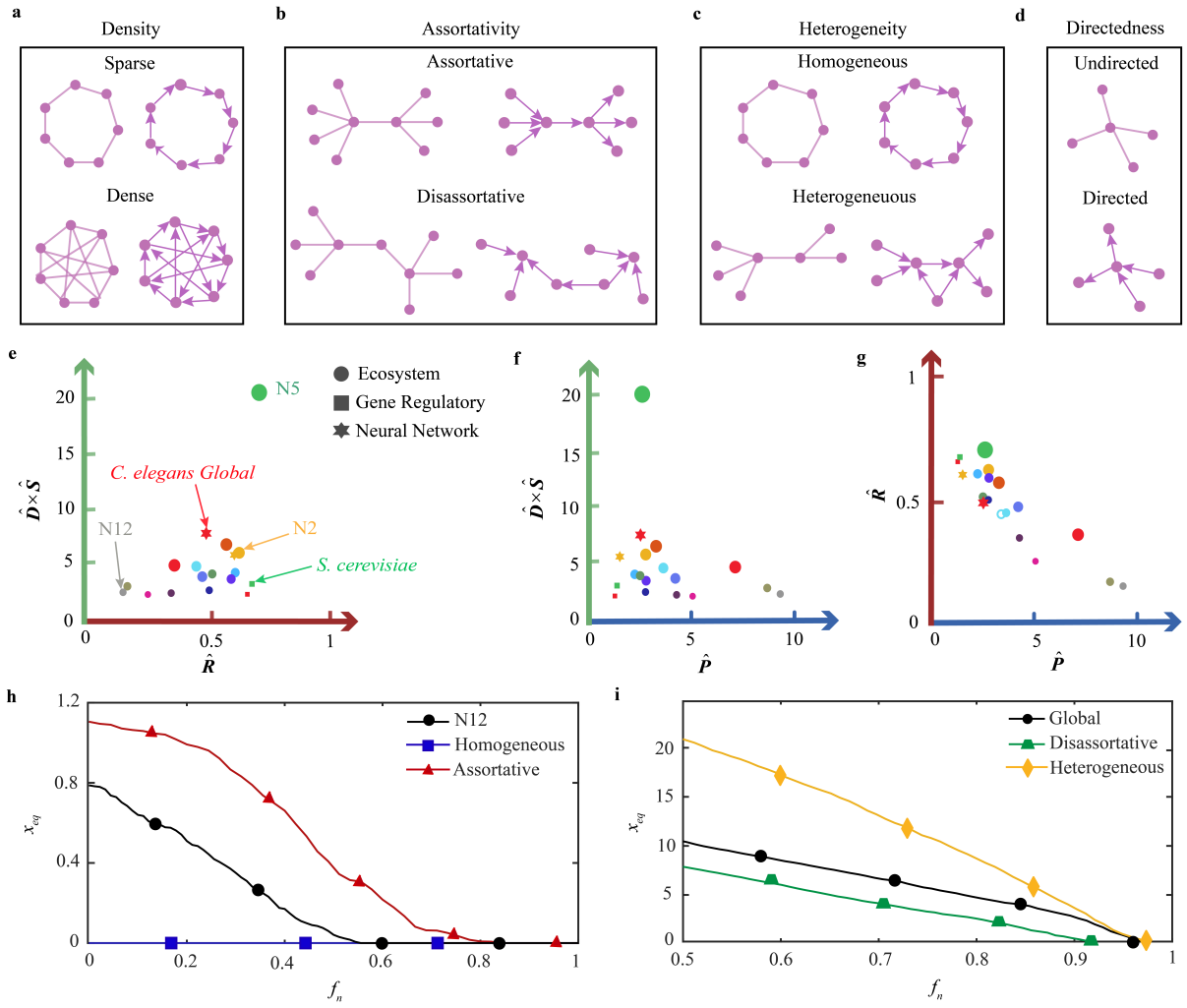

Figure 4: **The decomposition of k_{eq} and the impact of topological characteristics on network resilience**. The parameter k_{eq} is decomposed into four topological characteristics, namely **a,** Density $\hat{\boldsymbol{D}}$; **b,** Assortativity $\hat{\boldsymbol{R}}$; **c,** Degree heterogeneity $\hat{\boldsymbol{P}}$; and **d,** Directedness $\hat{\boldsymbol{S}}$. **e-g,** The four characteristics of ecological, gene regulatory and brain neural networks are displayed in three 2D plots to illustrate the sources of the resilience of each network, where the coordinates correspond to $\hat{\boldsymbol{D}} \cdot \hat{\boldsymbol{S}}$, $\hat{\boldsymbol{R}}$ and $\hat{\boldsymbol{P}}$ respectively. The color of the marker represents a specific network that matches the color of the networks in Fig. 2 and 3. Resilience of the network is proportional to the marker size. **h,** Using the mutualistic dynamical equation, x_{eq} vs. the fraction f_n of species removed are calculated from 100 realizations for real ecological network N12, the assortative N12, and the homogeneous N12; the curves are the average of the 100 realizations. Real network N12 remains uncollapsed until f_n = 60% of species are removed. The assortative N12 does not collapse until f_n = 80%; the homogeneous N12 is always collapsed. **i,** Using brain neural dynamics, x_{eq} vs. fraction f_n of neurons removed are calculated from 100 realizations for real *C.elegans Global* network, the heterogeneous *C.elegans Global* and the disassortative *C.elegans Global*; the curves are the average of the 100 realizations. Real *C.elegans Global* network resists collapse until approximately 90% of neurons are removed; the heterogeneous *C.elegans Global* collapses at f_n = 93%; and the disassortative *C.elegans Global* avoids collapse up to f_n = 83%.

Supplementary Information Table 4-6.

We conducted several experiments to analyze the impacts of the four topological characteristics on network resilience. We constructed twelve networks and grouped them into five categories. The characterization of each network is provided in Supplementary Information Table 7. Dynamical equations of mutualistic, gene regulatory, and brain neural networks are used to test the resilience of these twelve networks. The responses of each network to perturbations are shown in Supplementary Information Fig. S12-S26. The results do not only demonstrate the predictive accuracy and consistency of our formulation regardless of the diversity of topological structures, but also justify the implication of Eq. (13) that assortative undirected networks (high $\hat{\boldsymbol{R}}$ and $\hat{\boldsymbol{S}}$ = 2) with greater degree heterogeneity and density (high $\hat{\boldsymbol{P}}$ and high $\hat{\boldsymbol{D}}$) are more resilient. Furthermore, the observations demonstrate that network resilience is invariant to network size. When subjected to small perturbations, undirected networks experience minimal resilience loss, while directed networks suffer sizable resilience loss.

In Supplementary Information, other applications, including two variants of high-dimensional dynamical equations for modeling resilience of mutualistic ecosystems (Supplementary Information IV) as well as the high-dimensional model for modeling the resilience of Internet with respect to information transmission rate (Supplementary Information VII), are empirically studied. Our method exhibits the generalized predictability for resilience even though those systems conform to different forms of dynamics. Finally, in the recognition that interaction strength A_{ij} can be derived from real observations instead of calculating from M_{ij}, we study the resilience behavior of complex weighted networks that have A_{ij} following a probability distribution[29–31]. Supplementary Information Fig. S27-S32 confirm that our method still predicts the resilience and collapse points of these weighted networks accurately.

Summary

We presented a universal analytical modeling method using a single parameter k_{eq} to predict resilience of diverse dynamic systems with complex interactions among networked components. Formulation of k_{eq} is attributed to the nature of the interaction structure in the $N \times N$ space, and its predictive effectiveness is universal across differ-

ent network topologies. The changes caused by disruptive perturbations in the topological structure of networked components can be effectively accounted for by k_{eq}; this study confirms its effectiveness in predicting resilience of diverse complex systems in compliance with different interaction patterns. Furthermore, the predictive power of k_{eq} remains the same in complex networks with a wide variety of topological structures. By quantitatively decomposing k_{eq}, four topological characteristics, namely, density, assortativity, heterogeneity and directedness, are found to be the determinants of network resilience. We observe that resilient systems can withstand severe perturbations generally have large k_{eq} values. Our thorough analyses further complement the analytical understanding of systemic resilience [1,10,32].

Since our formulation is universally applicable to characterize and predict resilience of diverse complex systems, its universality allows us to come up with effective strategies to avert collapse of complex systems. The insights gained from this study informs design for significant enhancement of system's resilience with low systemic risk of collapse. These insights further provide design principles for resilience of a wide spectrum of realistic systems ranging from ecosystem [33,34] and biological networks [18,23,35] to technological infrastructures [36,37] and economic systems [19,38,39].

References

1. Jianxi Gao, Baruch Barzel, and Albert-László Barabási. Universal resilience patterns in complex networks. *Nature*, 530(7590):307, 2016.

2. Crawford S Holling. Resilience and stability of ecological systems. *Annual review of ecology and systematics*, 4(1):1–23, 1973.

3. Junjie Jiang, Zi-Gang Huang, Thomas P Seager, Wei Lin, Celso Grebogi, Alan Hastings, and Ying-Cheng Lai. Predicting tipping points in mutualistic networks through dimension reduction. *Proceedings of the National Academy of Sciences*, 115(4):E639–E647, 2018.

4. Mark Newman. *Networks*. Oxford university press, 2018.

5. Flaviano Morone, Gino Del Ferraro, and Hernán A Makse. The k-core as a predictor of structural collapse in mutualistic ecosystems. *Nature Physics*, 15(1):95, 2019.

6. Lei Dai, Daan Vorselen, Kirill S Korolev, and Jeff Gore. Generic indicators for loss of resilience before a tipping point leading to population collapse. *Science*, 336(6085):1175–1177, 2012.

7. Réka Albert, Hawoong Jeong, and Albert-László Barabási. Error and attack tolerance of complex networks. *nature*, 406(6794):378, 2000.

8. Samir Suweis, Filippo Simini, Jayanth R Banavar, and Amos Maritan. Emergence of structural and dynamical properties of ecological mutualistic networks. *Nature*, 500(7463):449, 2013.

9. Mark Ed Newman, Albert-László Ed Barabási, and Duncan J Watts. *The structure and dynamics of networks.* Princeton university press, 2006.

10. Mark EJ Newman. Assortative mixing in networks. *Physical review letters*, 89(20):208701, 2002.

11. Mengkai Xu, Srinivasan Radhakrishnan, Sagar Kamarthi, and Xiaoning Jin. Resiliency of mutualistic supplier-manufacturer networks. *Scientific reports*, 9(1):1–10, 2019.

12. Robert M May. Will a large complex system be stable? *Nature*, 238(5364):413, 1972.

13. Royce Francis and Behailu Bekera. A metric and frameworks for resilience analysis of engineered and infrastructure systems. *Reliability Engineering & System Safety*, 121:90–103, 2014.

14. Sergey V Buldyrev, Roni Parshani, Gerald Paul, H Eugene Stanley, and Shlomo Havlin. Catastrophic cascade of failures in interdependent networks. *Nature*, 464(7291):1025, 2010.

15. Marten Scheffer, Jordi Bascompte, William A Brock, Victor Brovkin, Stephen R Carpenter, Vasilis Dakos, Hermann Held, Egbert H Van Nes, Max Rietkerk, and George Sugihara. Early-warning signals for critical transitions. *Nature*, 461(7260):53, 2009.

16. Marten Scheffer, Stephen R Carpenter, Timothy M Lenton, Jordi Bascompte, William Brock, Vasilis Dakos, Johan Van de Koppel, Ingrid A Van de Leemput, Simon A Levin, Egbert H Van Nes, et al. Anticipating critical transitions. *science*, 338(6105):344–348, 2012.

17. Stefano Allesina and Si Tang. Stability criteria for complex ecosystems. *Nature*, 483(7388):205, 2012.

18. Katharine Z Coyte, Jonas Schluter, and Kevin R Foster. The ecology of the microbiome: networks, competition, and stability. *Science*, 350(6261):663–666, 2015.

19. Andrew G Haldane and Robert M May. Systemic risk in banking ecosystems. *Nature*, 469(7330):351, 2011.

20. Baruch Barzel and Albert-László Barabási. Universality in network dynamics. *Nature physics*, 9(10):673, 2013.

21. J Jelle Lever, Egbert H van Nes, Marten Scheffer, and Jordi Bascompte. The sudden collapse of pollinator communities. *Ecology letters*, 17(3):350–359, 2014.

22. Rudolf P Rohr, Serguei Saavedra, and Jordi Bascompte. On the structural stability of mutualistic systems. *Science*, 345(6195):1253497, 2014.

23. Uri Alon. *An introduction to systems biology: design principles of biological circuits*. Chapman and Hall/CRC, 2006.

24. Frank P Kelly, Aman K Maulloo, and David KH Tan. Rate control for communication networks: shadow prices, proportional fairness and stability. *Journal of the Operational Research society*, 49(3):237–252, 1998.

25. Socorro Gama-Castro, Verónica Jiménez-Jacinto, Martin Peralta-Gil, Alberto Santos-Zavaleta, Mónica I Peñaloza-Spinola, Bruno Contreras-Moreira, Juan Segura-Salazar, Luis Muniz-Rascado, Irma Martinez-Flores, Heladia Salgado, et al. Regulondb (version 6.0): gene regulation model of escherichia coli k-12 beyond transcription, active (experimental) annotated promoters and textpresso navigation. *Nucleic acids research*, 36 (suppl_1):D120–D124, 2008.

26. Haim Sompolinsky, Andrea Crisanti, and Hans-Jurgen Sommers. Chaos in random neural networks. *Physical review letters*, 61(3):259, 1988.

27. Marcus Kaiser and Claus C Hilgetag. Nonoptimal component placement, but short processing paths, due to long-distance projections in neural systems. *PLoS computational biology*, 2(7):e95, 2006.

28. Rolf Kötter. Online retrieval, processing, and visualization of primate connectivity data from the cocomac database. *Neuroinformatics*, 2(2):127–144, 2004.

29. Alain Barrat, Marc Barthelemy, Romualdo Pastor-Satorras, and Alessandro Vespignani. The architecture of complex weighted networks. *Proceedings of the national academy of sciences*, 101(11):3747–3752, 2004.

30. J Nathaniel Holland, Donald L DeAngelis, and Judith L Bronstein. Population dynamics and mutualism: functional responses of benefits and costs. *The American Naturalist*, 159(3):231–244, 2002.

31. Elisa Thébault and Colin Fontaine. Stability of ecological communities and the architecture of mutualistic and trophic networks. *Science*, 329(5993):853–856, 2010.

32. Seyedmohsen Hosseini, Kash Barker, and Jose E Ramirez-Marquez. A review of definitions and measures of system resilience. *Reliability Engineering & System Safety*, 145:47–61, 2016.

33. Jordi Bascompte, Pedro Jordano, Carlos J Melián, and Jens M Olesen. The nested assembly of plant–animal mutualistic networks. *Proceedings of the National Academy of Sciences*, 100(16):9383–9387, 2003.

34. Toshinori Okuyama and J Nathaniel Holland. Network structural properties mediate the stability of mutualistic communities. *Ecology Letters*, 11(3):208–216, 2008.

35. Vanni Bucci, Serena Bradde, Giulio Biroli, and Joao B Xavier. Social interaction, noise and antibiotic-mediated switches in the intestinal microbiota. *PLoS computational biology*, 8(4):e1002497, 2012.

36. Reuven Cohen, Keren Erez, Shlomo Havlinl, Mark Newman, Albert-László Barabási, Duncan J Watts, et al.

Resilience of the internet to random breakdowns. In *The Structure and Dynamics of Networks*, pages 507–509. Princeton University Press, 2011.

37. Radu F Babiceanu and Remzi Seker. Big data and virtualization for manufacturing cyber-physical systems: A survey of the current status and future outlook. *Computers in Industry*, 81:128–137, 2016.

38. Stefano Battiston, Guido Caldarelli, Co-Pierre Georg, Robert May, and Joseph Stiglitz. Complex derivatives. *Nature Physics*, 9(3):123–125, 2013.

39. Charles Perrings. Resilience in the dynamics of economy-environment systems. *Environmental and Resource Economics*, 11(3):503–520, 1998.

Acknowledgments

Author Contributions

All authors designed and performed the research. M.X. performed the numerical calculations and analyzed the empirical data. S.K., X.J., S.R. and M.X. wrote the manuscript and designed the figures.

Competing Interests

The authors declare no competing interests.

Additional Information

Supplementary information accompanies this paper.

Methods

In general, the interaction strengths A_{ij} between nodes in complex systems are directed and weighted, indicating that the impact of node i on node j is different from the impact of node j on node i[1,17,29]. The heterogeneity of

interaction strengths is intrinsically related to the resilience of complex systems, and strengths A_{ij} can be expressed as adjacency matrix M_{ij} [1,22], whose elements take the value 1 if a link connects node i to node j and 0 otherwise. Therefore, this work studies the impact of statistical properties of topological structure M_{ij} on the resilience of systems governed by equation (1).

For resilience prediction, the weighted interactions A_{ij} are replaced by M_{ij} to generalize the representation of interaction structures of complex systems. By assuming that the degree correlations for all connected nodes are identical, the interaction for each node i $\sum_{j=1}^{N} M_{ij} Q\left(x_i, x_j\right)$ in high-dimensional dynamical Eq. (1) is reduced to $Q\left(x_{eq}, k_{eq}\right)$ in uni-dimensional Eq. (3) through linear approximation (see Supplementary Section II for details). Through stability analysis, the resilience of the system represented by the feasible solution x_{eq}^{c} is derived by equation (5). Here, feasible means that x_{eq}^{c} must be non-negative because the states of nodes can not be negative [1,15,16]. A resilient system must have a nontrivial solution $x_{eq}^{c} > 0$, indicating that there exists a minimum condition of total interactions rooted in the topological structure of a system to maintain its resilience. Our endeavours reside in systematically studying how the topological properties affect the resilience loss and tipping point of systems with miscellaneous structures.

We analyze the resilience of weighted complex systems spanning from mutualistic, gene regulatory, brain neural and Internet networks subjected to different levels of realistic perturbations. Parameters of resilience functions governing different systems are obtained from field data reported in literature [1,3,5]. The severity of realistic perturbations is represented by a fraction f_n of nodes removed from the system. The system resilience x_{eq}^{c} is derived in the perturbation process. To validate the prediction accuracy and consistency of our formulation, the resilience calculated by Eq. (1) is treated as the ground truth, and the resilience calculated by Eq. (5) is as estimate. It is found that a feasible, stable and non-trivial solution exists only when $k_{eq} > k_{eq}^{c}$. By contrast, x_{eq}^{c} is always 0 when $k_{eq} < k_{eq}^{c}$, meaning that the system is in the collapsed state. Comparisons performed in Fig.2 and Fig.3 between numerical results demonstrate a good agreement between the results provided by the high-dimensional model and our formulation. It is worth noting that k_{eq}^{c} is invariant for one specific system even though the system has networks exhibiting diverse topological structures. Resilient systems generally have large k_{eq} values, which

are much greater than the tipping point k_{eq}^{c}. The statistical decomposition on k_{eq} unveils that it is determinately explained by the product of four topological characteristics : density, assortativity, heterogeneity, and directedness as shown in Eq. (13). In summary, each characteristic contributes to the high resilience of a system.

In Supplementary Information IX, the predictability of our formulation is validated on Erdős Rényi and scale-free networks constructed for a wide range of parameters, which cover broad degree distributions in realistic networks. The analytical results presented in Supplementary Information X show consistent and good predictive performance of our formulation on realistic weighted networks (Erdős–Rényi and scale-free networks with the uniform distribution of strengths[5]).

Data Availability

Data that support the findings of the studies are publicly available at the web https://github.com/Mengkai-Source.

Supplementary Files

This is a list of supplementary files associated with this preprint. Click to download.

- SupplementaryInformation.pdf